A NEW EFFECTIVE $K_7SrY_2B_{15}O_{30}$: Eu^{3+} SAMPLE FOR WHITE LEDS YIELDING NON-DOSAGE ABATEMENT AS WELL AS STRONG HEAT CONSISTENCY

Anh Tuan Le[1,*], *Hsiao-Yi Lee*[2]

[1]Faculty of Electrical and Electronics Engineering, Ton Duc Thang University, Ho Chi Minh City, Vietnam.
[2]Department of Electrical Engineering, National Kaohsiung University of Science and Technology, Kaohsiung, Taiwan.

*Corresponding Author: Anh Tuan Le (Email:leanhtuan1@tdtu.edu.vn)
(Received: 06-December-2023; accepted: 15-April-2024; published: 30-June-2024)
http://dx.doi.org/10.55579/jaec.202482.443

Abstract. *In this study, a unique high-temperature sintering process was used to create a red-emitting, non-dosage abatement $K_7SrY_{2-2x}B_{15}O_{30}$: xEu^{3+} (KSEBOE) ($0.1 \leq x \leq 1.0$) sample. The phosphors were suggested with the purpose of accomplishing warm and good-color-rendering white light for phosphor-conversion LED. By steadily increasing doping Eu^{3+} ions, $K_7SrY_2B_{15}O_{30}$ (KSEBO) may demonstrate impressive photoluminescent proficiency and the greatest discharge wavelength focalized under 617 nm. Additionally, the absence of dosage abatement may result from the large range (7.012 Å) among two Eu^{3+} granules. The phosphor exhibited great inner quantum yield (∼ 78.71%), superb hue clarity (∼88.32%), as well as potent heat consistency (with discharge intenseness under 140°C reaching nearly 97.31%). The strong white illumination yielding a low correlated chroma temperature (CCT) reaching 4211 K as well as chroma coordination shown as (0.3675, 0.3556) may be produced by covering $BaMgAl_{10}O_{17}$: Eu^{2+}, $(Ba, Sr)_2SiO_4$: Eu^{2+}, along with KSEBO above one n-UV chip. The KSEBO phosphor also demonstrated notable n-UV/blue-light scattering performance, especially at high doping concentrations (30-40%), enabling its potential to improve the color uniformity of the white LED. Shortly, the non-dosage abatement KSEBOE molecule possesses a strong chance of being a red phosphor sample for the solid-state illumination industry.*

Keywords: *Photoluminescence; Eu^{3+} granules; solid-state reactivity; WLED apparatus derived from red phosphor samples.*

1. Introduction

Owing to their benefits of great effectiveness, light level, reliability, safety, as well as power conservation, white light-emitting diodes (WLEDs) have emerged as a standard illumination apparatus meant for worldwide carbon neutralization [1, 2]. Normally, a yellow commercial $Y_3Al_5O_12$: Ce^{3+} sample is coated on one blue InGaN chip to create a WLED. Due to the absence of a red element in the spectrum, the considerable CCT as well as low chroma rendition index (CRI) would restrict employment, particularly when it comes to interior illumination as well as screens [3]. One way to get around these

drawbacks is to add red phosphor samples subject to excitation through blue LED chips [4]. As an alternative, trichromatic phosphors can be combined with near-ultraviolet chips to produce high-quality white illumination emission. Because red phosphor is invisible to human sight, it seems especially crucial to produce red emitting phosphor in comparison to green and blue phosphors. The light field is currently dominated by red phosphor samples derived from nitride as well as sulfide, but their widespread use is restricted by the chemical as well as physical unreliability in sulfides along with the difficult manufacturing criteria for nitrides. Thus, the creation of innovative, highly bright and stable n-UV or blue-illumination-driven red phosphor samples is essential [5, 6].

Rare-earth ion doped phosphors have received a lot of attention recently due to their benefits, including brilliant, visible emissions, adjustable emission bands, and ease of production [7, 8]. The $^5D_0 \rightarrow {}^7F_2$ transition can be attributed to the intense red-light emission that Eu^{3+} ions can produce among the rare-earth ions. This emission occurs at roughly 610 nm. The phosphor bases impact the amplitude of the CSB strength, and the formation surrounding the Eu^{3+} granules would alter the shift strength proportion for the electrical dipole to the magnetic dipole [9–11]. Hence, for Eu^{3+} ion doping, picking the right host is essential. As of now, inorganic substances such as oxides, borates, molybdates, phosphates, as well as fluorides have been chosen as luminous hosts. Borates, in contrast, have acceptable chemical as well as physical reliability along with a small level for manufacture processes, making them an appropriate host for rare-earth ions [12–16]. A new $Ca_3Lu(AlO)_3(BO_3)_4$ sample yielding significant quantum effectiveness as well as good hue clarity was described by Huang *et al.* [17]; however, the severe heat degradation is unsatisfactory. High-quantum efficiency $Ca_3Eu_2B_4O_{12}$ phosphor with non-concentration quenching was reported by Li *et al.* [18], but its temperature stability was universal. Eu^{3+} doped $YGa_3(BO_3)_4$ phosphors show excellent heat stability, according to Lu *et al.* [19], although the illumination mechanism is yet unknown. There are not many investigations on Eu^{3+} doped borate materials that may not concentrate. The non-concentration quenching specimens' examination of their luminescence characteristics is unclear, and their thermal stability is not especially good either. Finding non-concentration quenching red phosphors that are ideal for this purpose and have great hue purity, high brightness, and thermal stability is crucial. The elevated inner quantum effectiveness ($\sim 78.71\%$), outstanding hue clarity ($\sim 88.32\%$), as well as solid heat consistency when subject to the radioactivity reaching 393 nm may enable a phosphor's implementation within WLED apparatuses. The study herein concerns a red $K_7SrY_{2-2x}B_{15}O_{30}$: xEu^{3+} (KSYBO: xEu^{3+}) ($0.1 \leq x \leq 1.0$) sample yielding non-dosage abatement. One possible option for an illuminating gadget is one WLED enclosed using a UV chip along with $K_7SrY_{2-2x}B_{15}O_{30}$ (KSEBO) phosphor.

2. Method

2.1. Phosphor synthesis and characterization

The intricate XRD behavior for the Eu^{3+} incorporated and undoped KSYBO samples along with the KSYBO canon readings have been demonstrated. The fact that it is possible to fit the solid solution's diffraction peaks to the $K_7SrY_2B_{15}O_{30}$ canon XRD behavior and that contamination is not discovered suggests that the whole hard compound may seldom cause a revolution in the crystal structure [20]. Also, the foundation for the impressive optic performance will be set by the total substitution of Y^{3+} ions. The first model presented by Mutailipu's work was utilized for rectifying the KSYBO base as well as KSEBO via the GSAS software in order to better examine the stage clarity as well as corroborate the formation for the KSYBO base. The results of the fitting, the locations of the Bragg diffraction peaks, and the discrepancy among the calculated and observed findings are shown. The refinement's detailed information reveals that the powder was obtained, crystallizing within one trigonal formation accompanied by an R32 space group [21]. Also, the low determined/profile R-elements (R_{wp} val-

ues of 10.36%, 10.94%, R_p values of 7.76%, 8.36%,) along with x2 values of 1.50, 1.97 points to the creation of the clarified stage accompanied by accurate structural data supporting additional research. The KSYBO: Eu^{3+} picture was obtained using scanning electron microscopy (SEM). The synthesized sample exhibits a wide particle size range, ranging from $5 \sim 10$ μm, and an uneven shape.

The YAG:Ce nano-sized particles were prepared with sol-gel technique without additives [22]. The obtained phosphor possesses a size of about 3-4 microns and a nearly spherical shape. The preparation route can be summarized as follows. Initially, the raw yttrium oxide and cerium nitrate hexahydrate were dissolved in aluminum nitrate nonahydrate solution (60 mL). The produced solution was then continuously stirred and heated at 80 degrees Celsius, followed by a two-hour evaporation phase to get a gel form. Next, the gel underwent a drying phase for five hours at 120 degrees Celsius. The obtained product was subsequently subjected to a calcination process in a reduced atmosphere for three hours at 1550 degrees Celsius.

2.2. WLED simulation

The yellow phosphor mixture YAG:Ce^{3+} is combined with a number of LED chips to make the LED model. Figure 1 provides an illustration of the LED model. Figures 1b, 1c, along with 1d, display bonding as well as element organization diagrams, whereas Figure 1a displays the constructed model of the LED used in this work. Figure 1d also shows the 3D simulation model made with the LightTools program.

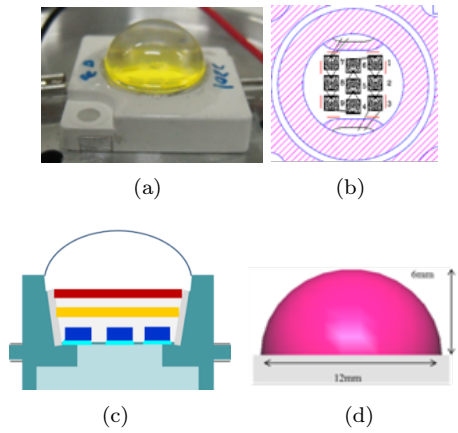

Fig. 1: WLEDs setting: (a) WLED device, (b) Binding graph, (c) WLED's graphical depiction, (d) WLED recreated via LightTools.

3. Results and discussion

3.1. Computation

It is clear that the structure is made up of YO_6, SrO_6, as well as $KO_{6/8}$ corner-shared polyhedrons. Eight, eight, and six O^{2-} ions coordinate the three K^+ sites to produce deformed polyhedra with precise bond lengths. The selective occupancy in Eu^{3+} from KSYBO is examined in order to ascertain the photoluminescence variation of Eu^{3+}. The study demonstrates that the percent aberration for radius disparity remains below 30% according to Davolos' calculation of the percentage of radius difference (Dr) [23]:

$$Dr = 100^* \frac{R_m(CN) - R_d(CN)}{R_m(CN)} \qquad (1)$$

The cation and activator radius are represented by the symbols Rm (CN) and Rd (CN). With computation involving the radii for K^+(1.38 Å (CN = 6) and 1.51 Å (CN = 8)), Sr2+ (1.18 Å (CN = 6)), Y^{3+} (0.9 Å (CN = 6)) and Eu^{3+} (0.947 Å (CN = 6)) accompanied by various coordinates, the percent difference among Eu^{3+} as well as K1, K2, K3, Sr, Y reaches approximately 29.4 %, 31.4 %, 19.7 % and 5.2 %, respectively. It is known that Eu^{3+} benefits from occupying Y^{3+} cation sites by combining with various cations' valences.

The KSYBO and KSEBO diffuse reflectance spectra (DRS) range from the UV to the visible area. Both KSYBO and KSEBO exhibit the same broad absorption peak of about 225 nm, indicating the peak is a result of host absorption. The charge shift band (CSB) for Eu^{3+}-O^{2-} as well as the distinctive shift for $^7F_0 - {}^5L_6$ and $^7F_0 - {}^5D_2$ can be attributed to the wide band under 250 nm as well as the sharp bands under 393 as well as 467 nm for the KSEBO specimen.

The Kubelka-Munk calculation will be employed for assessing the optical band gap (Eg), based on the DRS of KSYBO [24]:

$$[F(R_\infty)hv]^n = A(hv - Eg) \tag{2}$$

A stands for the proportional constant. hv signifies photon power. The formula is (R_∞), where R is the absorption coefficient divided by the reflection coefficient. The computed Eg of KSYBO is ∼4.192 eV, demonstrating its aptitude when it comes to rare-earth incorporation. The electrical structure and status denseness (SD) would be computed concurrently using the first principles theory [25]. A direct bandgap substance called KSYBO has one bandgap reaching approximately ∼ 4.384 eV, which is comparable to the observed optical bandgap. The total DOS of KSYBO and the fractional state denseness (FSD) interacting with the intrinsic K, Sr, Y, B, as well as O granules are displayed. The p orbitals for O (2p) as well as the p trajectories for B make up the majority of the valence band's top (VB) structure (2p). The Sr (3d) orbitals contribute little to the lowest point for the conducting band, which primarily contains B (2p) as well as Y (4d) trajectories. The large direct band gap for KSYBO suggests that this phosphor base can be doped with Eu^{3+} granules.

The red KSEBO treated with 393-nm CIE chromaticity diagram is provided. KSEBO specimens' coordinates are shown in the red area at (0.6381, 0.3615). The KSYBO: xEu^{3+} specimen's chroma coordinates were measured at 393 nm of illumination. The specimen's CIE coordinates modestly changed in the red area when Eu^{3+} doping dosage increased. A further indication of the phosphor's great hue stability is that the coordinates for KSEBO specimens were slightly altered while being heated, from (0.6179, 0.3816) under 20^{o}C into (0.6136, 0.3858) under 230^{o}C. Equation 3 can be used to assess the emitting hue purity for narrow-band illumination sources as an indicator of the hue emitting properties [25].

$$Color\ purity = \frac{\sqrt{(x-x_i)^2 + (y-y_i)^2}}{\sqrt{(x_d-x_i)^2 + (y_d-y_i)^2}} \times 100\% \tag{3}$$

(x, y) are the specimen's CIE coordinates; (x_i, y_i) signifies the luminous points; the illumination's coordinates are (0.3101, 0.3162). (x_d, y_d) signifies the prevalent wavelength coordinates. The synthetic specimens exhibit a high degree of hue purity.

Evidence that there is no luminous dosage quenching event may be found in the transient spectrum for KSYBO: Eu^{3+} phosphors. The singular-exponential expression may effectively fit every degradation arch, and it correlates with the Eu^{3+} dosage in the KSYBO: Eu^{3+} for the room temperature PL lifetime [26]:

$$I(t) = I_0 + A\exp(-t/\tau) \tag{4}$$

where I_0 signifies the baseline rectification. A signifies one constant. t signifies the excitation status period, and $I(t)$signifies the discharge intenseness. Through the mentioned factors for KSYBO: xEu^{3+}, the median degradation duration's reach around 5.0485, 5.0103, 4.9438, 4.8302, 4.6698, and 4.5280 ms with x values of 0.1, 0.3, 0.5, 0.7, 0.9, and 1.0. The findings demonstrate that the predicted t values lie within the typical Eu^{3+}-activated phosphor microsecond range, confirming that the emissions are spin prohibited. More necessary, the fluorescent durations for KSYBO: xEu^{3+} were practically constant, showing that dosage abatement was non-existent, for $x = 0.1 - 1.0$.

Equation 5 is used to compute the activation energy and further describe the specimens' heat quenching behavior [27]:

$$I(T) = \frac{I_0}{1 + c\exp\left(-\frac{\Delta E}{kT}\right)} \tag{5}$$

I_0 and $I(T)$ signify the initial intenseness as well as intenseness based on heat level, respectively, whereas ΔE stands for trigger power. k signifies the Boltzmann constant. Through computation, ΔE reached approximately 0.172 eV via the linear fitting results for $\ln[(I_0/I_T)-1]$ versus $1/kT$.

$BaMgAl_{10}O_{17}$: Eu^{2+}, $(Ba, Sr)_2SiO_4$: Eu^{2+}, along with KSEBO samples would be merged for the task of creating WLED apparatuses in order to assess the possible applications of KSEBO phosphors. The WLED device's electroluminescence (EL) spectrum, prepared at one conducting current measured at 20 milliamperes. The

CCT for bright white light is 4211 K accompanied by hue coordinate (0.3675, 0.3556). Apparently, KSYBO: Eu^{3+} would be appropriate in warm WLED apparatuses.

Besides, for assessing specific the performance of KSEBO phosphor, the YAG:Ce^{3+} is solely used to combine with the KSEBO phosphor to reduce the simulation complexity. The results also provide valuable data for improving the commercial WLED with YAG:Ce^{3+} phosphor as the active-conversion layer. The detailed discussion of the simulation and test results as a function of varying KSEBO concentrations is demonstrated in the next section.

3.2. The effect of phosphor on WLED performance

There are two dominated components in the PLE spectrum, including CTB and internal shifts for Eu^{3+} granules between 310 and 500 nm, as well as all the excitation peaks. These components can also be successfully suited to the DRS. Particularly, the transition of $^7F_0$ to the $^5H_6$, $^5D_4$,$^5G_4$, $^5G_2$, $^5L_6$, $^5D_3$, and $^5D_2$ levels can be attributed to the abrupt apexes under 321, 362, 380, 385, 393, 416, and 467 nm, respectively. The n-UV region's greatest stimulation peak at 393 nm makes it suitable for use in the form of an effective red phosphor in n-UV LED chips. Sharp apexes appear under 578, 590, 617, 652, as well as 685 nm when 393 nm radiation exits the material. These peaks are associated with the internal shifts for Eu^{3+} granules from $^5D_0$ to ^7F_j (j values of 0, 1, 2, 3, 4). Since the crystal field cannot affect the split of the $^5D_0 \rightarrow {}^7F_0$ transition, the quantity of discharge apexes associated with the $^5D_0 \rightarrow {}^7F_0$ transition matches the number of different positions. The presence of an independent peak among the emission peaks associated with the $^5D_0 \rightarrow {}^7F_0$ transition demonstrates that that Eu^{3+} ions take the place of Y^{3+} ones.

The concentration quenching effect will have a significant impact on the emitting strength for samples subject to rare-earth incorporation. On the other hand, with KSYBO: Eu^{3+} phosphors, it is safe to disregard the dosage abatement. KSYBO: xEu^{3+}'s PL strength varies according to the amount of Eu^{3+} ions doped in it ($0.1 \leq x \leq 1.0$). Thus, rising doping levels only affect emitting strength and have no effect on the shift in emission peaks. The emission intensity reaches its peak when Eu^{3+} completely replaces Y^{3+} granules (x = 1.0).

The dosage abatement influence may generally result from the greater likelihood for radiative (so-called photon exchange) and non-radiative (caused by small-span reciprocations or extensive-span multi-pole interactivities) power transmission processes between luminous centers. Consequently, as the range among the luminescent focal points decreases, the dosage quenching effect will become more apparent. According to Blasse, exchange interactions will occur during the power transmission process across a distance of less than 5 Å. On the other hand, the multipolar interactions will be considerable if the separation among Eu^{3+} ions is greater than 5 Å, but in comparison to the exchange interaction effect, they will have a minor impact on the power transfer process. The smallest separation among two Eu^{3+} ions in the KSEBO structure is determined to be 7.012 Å, which is significantly greater than the distances between the closest Eu^{3+} ions in LaSc3(BO3)4, Ba6Gd2Ti4O17, and K5Y (P2O7), which are respectively 6.22 Å, 5.93 Å, and 5.6 Å. Also, all of the phosphors stated above can show the non-dosage abating activity, indicating that one sufficiently extensive range would be advantageous for significant incorporating dosages as well as the phosphors' terminal discharge intensities.

The red/orange proportion, or the proportion for the $^5D_0$ - $^7F_2$ emitting strength to the $^5D_0$ - $^7F_1$ emitting strength, is determined to ascertain the preference of the Eu^{3+} occupation. The orange percent would be between 580 and 600 nm for integral potency. The red percent would be between 603 and 630 nm. The red percent would be between 500 and 750 nm in integral potency proportion. Said proportion was slightly altered when Eu^{3+} doping concentration increased (R/O $\approx$ m2), which is within the allowed error range, indicating that it occupied the Y^{3+} site.

The scattering factor of light emission as a function of KSYBO: Eu^{3+} dose is shown in Fig. 2. By increasing the amount of KSYBO: Eu^{3+} used, the effectiveness of light transmission and wavelength conversion can be improved. Furthermore, an increase in forward emission blue light diffusion and a decrease in blue light scattering and reabsorption can result in increased brightness. To do this, less yellow phosphor, or YGA:Ce, is used, and more KSYBO: Eu^{3+} is used instead. Moreover, this lessens the variation in the related color temperature (CCT). While Fig. 3 demonstrates that the concentration of YGA:Ce declines with increasing KSYBO: Eu^{3+} dose, Figs. 4 and 5 demonstrate that CCT is concentration independent. Fig. 4 illustrates how greater doping may enable the phosphor to lower the variance in its CCT. In Fig. 5, the D-CCT eventually reaches its lowest value when KSYBO: Eu^{3+} is utilized with 40%, which is approximately 200 K lower than the result when 20% of KSYBO: Eu^{3+} is used.

As seen in Fig. 6, increasing the KSYBO: Eu^{3+} does not always lead to an increase in the brightness of the white light emission. The best results were obtained with 0-10% of KSYBO: Eu^{3+}, whereas the worst results were observed with 50% of KSYBO: Eu^{3+}. D-CCT at 40% of KSYBO: Eu^{3+}, where the reduction is greatest, is shown in Fig. 5. As a result of increased backscattering and reabsorption, this exhibits a weaker blue emission and an uneven color distribution. Higher KSYBO: Eu^{3+} dosages in particular would promote the light's conversion from blue to yellow or orange-red because the phosphor absorbs more backscattered blue light. After the KSYBO: Eu^{3+} concentration is high enough, the phosphor coating begins to expand. To put it another way, a high phosphor dose might increase the percentage of converted light that is back-reflected, which could decrease luminous intensity while increasing CCT. It was discovered that a KSYBO: Eu^{3+} ratio of 0 - 10% was the best one for improving brightness and color uniformity in the simulated WLED.

The KSYBO: Eu^{3+} concentration has a significant impact on the brightness and color rendering of white LEDs. With the weight of 50% KSYBO: Eu^{3+}, the hue rendering indicator (CRI) and hue quality scale (CQS) assessments of color rendition values showed a consistent reduction, see in 7 and 8. Unbalanced blue, green, and yellow-orange patterns may have contributed to the apparent drops in CRI and CQS. High KSYBO: Eu^{3+} dose results in increased dispersion and an irregular color of the light output, which leans more toward the yellow-orange region. Further study of particle size is needed to manage the CRI and CQS, which is what our future research investigation aims to do.

Figure 9 displays the emission spectra of the KSYBO: Eu^{3+}-based WLED. The ability of the phosphor to intensify blue and orange-red light was demonstrated by the whole spectrum of white emission. The characteristics of KSYBO: Eu^{3+} can be altered to alter the patterns of light scattering and absorption and increase lighting efficiency. The blue (450 nm) and yellow-orange (∼600 nm) ranges have the highest peaks.

4. Conclusions

In conclusion, a thorough study was done on the non-dosage abatement in $K_7SrY_{2-2x}B_{15}O_{30}$: xEu^{3+} solid-solution phosphors. The phosphor' CIE coordinates were (0.6381, 0.3615), and its chroma clarity reached roughly 88.32%, with an IQE reaching roughly 78.71%. In addition, KSEBO demonstrated strong heat consistency, with the PL discharge intenseness remaining under roughly 97.31% compared to its preliminary result under 140^{o}C. Additionally, to create a WLED apparatus yielding a small CCT, we placed $BaMgAl_{10}O_{17}$: Eu^{2+}, $(Ba, Sr)_2SiO_4$: Eu^{2+}, and KSEBO above an n-UV chip. The findings of the experiment indicate that the KSYBO: Eu^{3+} samples are candidates for use as red phosphors in WLED applications.

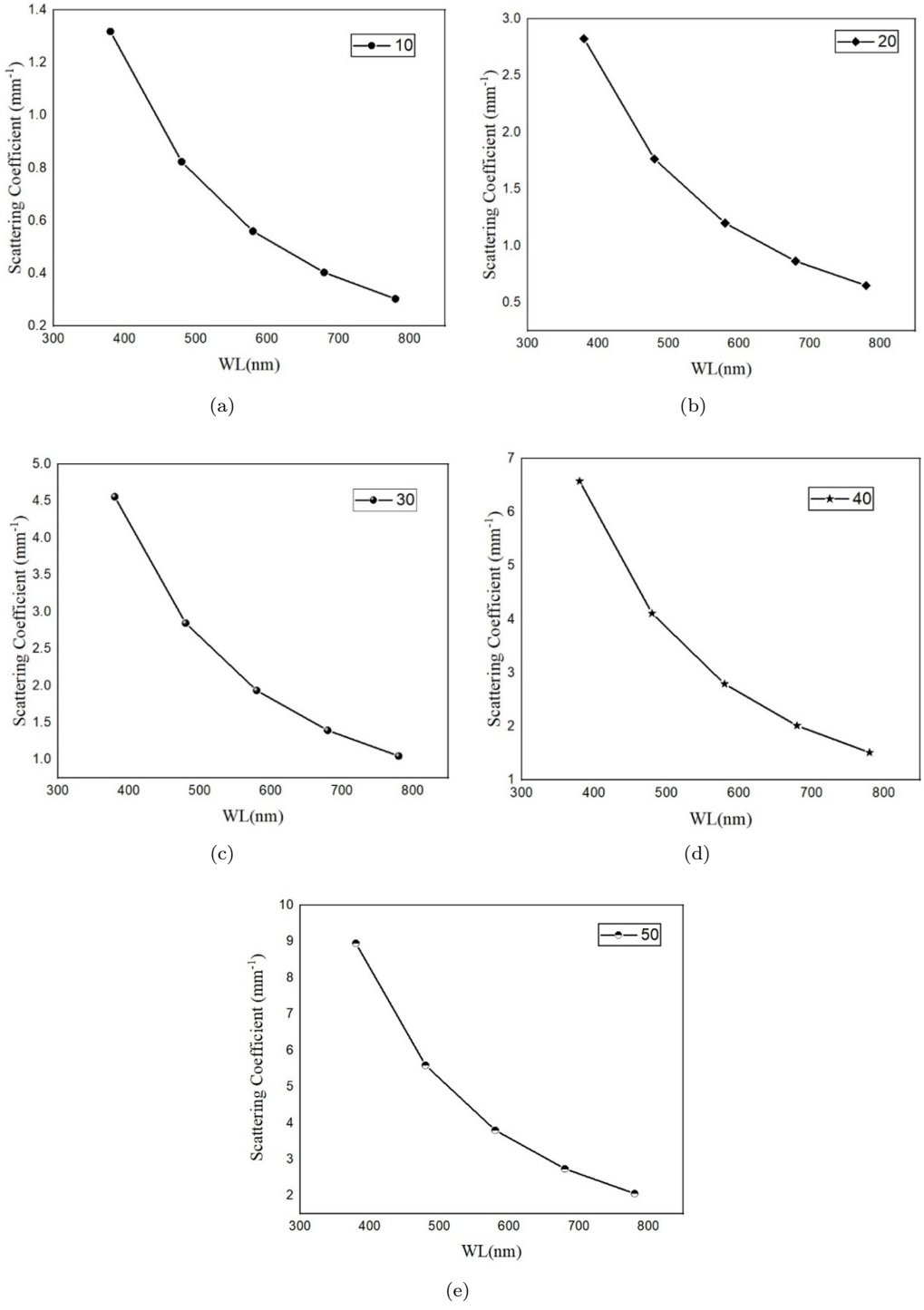

Fig. 2: Scattering coefficients according to various KSYBO: Eu^{3+} dosages: (a) 10%; (b) 20%; (c) 30%; (d) 40%; (e) 50%.

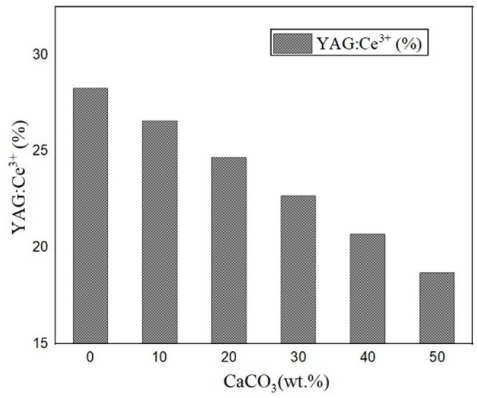

Fig. 3: YGA:Ce phosphor dosage values with different KSYBO: Eu^{3+} dosages.

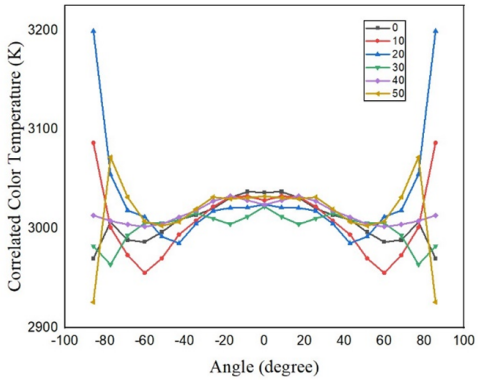

Fig. 4: Variation of CCT with various KSYBO: Eu^{3+} dosages.

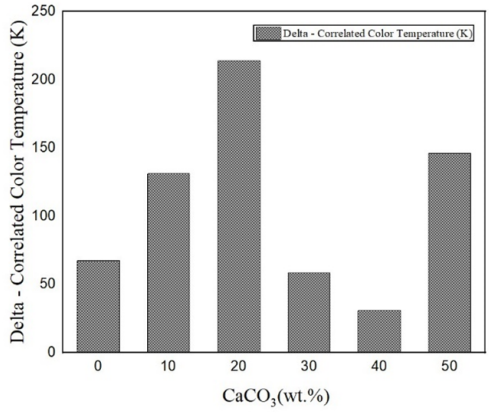

Fig. 5: Investigation of the color deviation changes with various KSYBO: Eu^{3+} dosages.

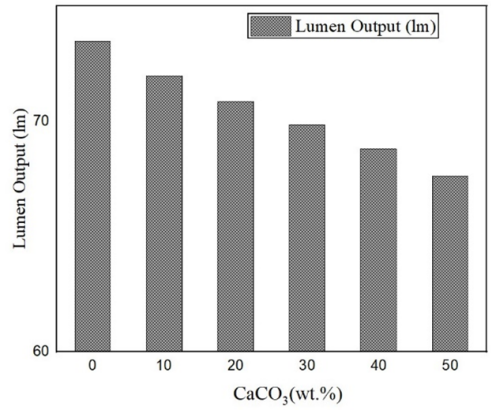

Fig. 6: Luminescence strength with various KSYBO: Eu^{3+} dosages.

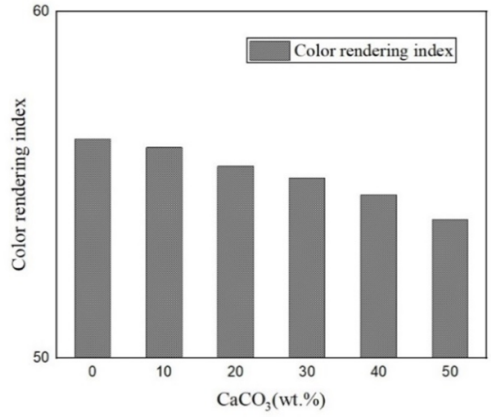

Fig. 7: CRI values of the WLED with various KSYBO: Eu^{3+} dosages.

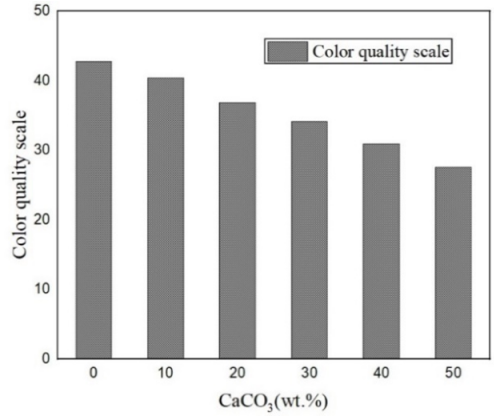

Fig. 8: CQS values with various KSYBO: Eu^{3+} dosages.

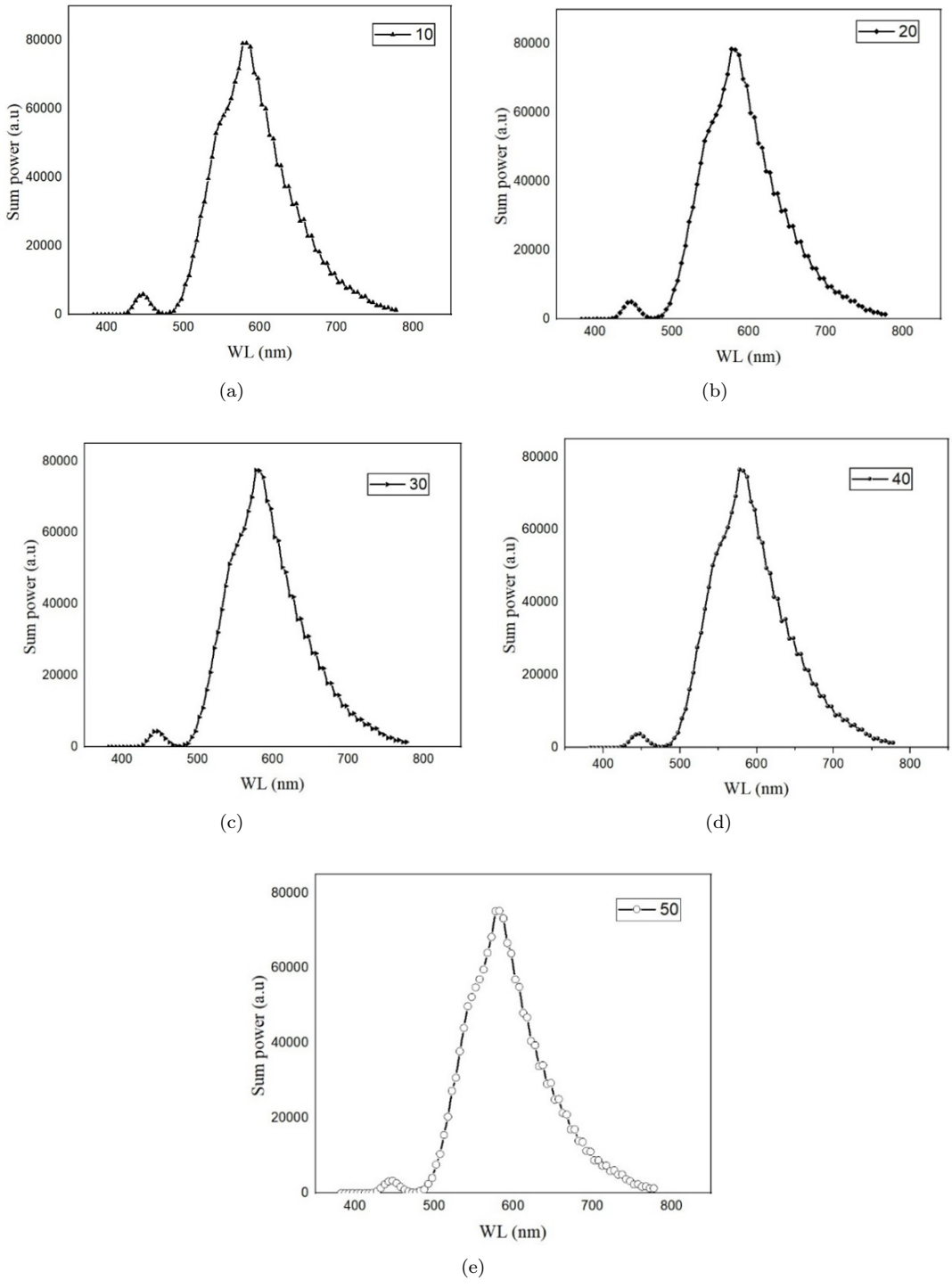

Fig. 9: Luminescence power of the WLED: (a) 10%; (b) 20%; (c) 30%; (d) 40%; (e) 50%.

References

[1] K. Orzechowski, M. M. Sala-Tefelska, M. W. Sierakowski, T.R. Woliński, O. Strzeżysz, and P. Kula. Optical properties of cubic blue phase liquid crystal in photonic microstructures. *Opt. Express*, 27:14270–14282, 2019.

[2] X. Yao, V. Pathak, H. Xi, A. Chaware, C. Cooke, K. Kim, S. Xu, Y. Li, T. Dunn, P. C. Konda, K. C. Zhou, and R. Horstmeyer. Increasing a microscope's effective field of view via overlapped imaging and machine learning. *Opt. Express*, 30:1745–1761, 2022.

[3] S. An, J. Li, X. Li, and Y. Su. Wftn ssb 16-qam signal transmission and direct detection based on tomlinson-harashima precoding with computed coefficients. *J. Light. Technol.*, 39:2059–2066, 2021.

[4] R. Deeb, J. V. D. Weijer, D. Muselet, M. Hebert, and A. Tremeau. Deep spectral reflectance and illuminant estimation from self-interreflections. *J. Opt. Soc. Am. A*, 36:105–114, 2019.

[5] W. Chang, Y. Kuo, Y. Kiang, and C. C. Yang. Simulation study on light color conversion enhancement through surface plasmon coupling. *Opt. Express*, 27:629–642, 2019.

[6] H. Cheng, S. Tong, X. Deng, J. Li, P. Qiu, and K. Wang. In vivo deep-brain imaging of microglia enabled by three-photon fluorescence microscopy. *Opt. Lett.*, 45:5271–5274, 2020.

[7] H. Jia, Q. J. Wu, C. Jiang, H. Wang, L. Q. Wang, J. Z. Jiang, and D. X. Zhang. High-transmission polarization-dependent active plasmonic color filters. *Appl. Opt.*, 58:704–711, 2019.

[8] D. M. Kustov, E. I. Kozlikina, K. T. Efendiev, M. V. Loshchenov, P. V. Grachev, Yu. S. Maklygina, I. S. Trifonov, A. V. Baranov, E. F. Stranadko, D. N. Panchenkov, V. V. Krylov, and V. B. Loschenov. Laser-induced fluorescent visualization and photodynamic therapy in surgical treatment of glial brain tumors. *Biomed. Opt. Express*, 12:1761–1773, 2021.

[9] Z. Song, Z. Song, J. Zhao, and F. Gu. Micrometer-level 3d measurement techniques in complex scenes based on stripe-structured light and photometric stereo. *Opt. Express*, 28:32978–33001, 2020.

[10] H. Zimmermann B. Waßmuth, G. W. Fuchs and T. F. Giesen. Concept and application of a linearized ring multipass optics configuration. *Appl. Opt*, 60:10273–10281, 2021.

[11] H. Zhang, Z. Zhang, X. Song, R. Zhao, Z. Zhang, D. Jia, and T. Liu. Design and characteristics of tunable in-plane optofluidic lens actuated by viscous force. *Opt. Lett.*, 46:4017–4020, 2021.

[12] V. Dumont, S. Bernard, C. Reinhardt, A. Kato, M. Ruf, and J. C. Sankey. Flexure-tuned membrane-at-the-edge optomechanical system. *Opt. Express*, 27:25731–25748, 2019.

[13] J. Jia, Y. Jiang, H. Gao, L. Zhang, and Y. Jiang. Three-wavelength passive demodulation technique for the interrogation of efpi sensors with arbitrary cavity length. *Opt. Express*, 27:8890–8899, 2019.

[14] A. J. Henning, J. Williamson, H. Martin, and X. Jiang. Improvements to dispersed reference interferometry: beyond the linear approximation. *Appl. Opt.*, 58:131–136, 2019.

[15] S. G. Bugoffa and M. R. Chatterjee. Electromagnetic and imaging properties of chiral dispersive spherical interfaces under bimodal propagation using abcd matrices. *Appl. Opt.*, 60:7804–7814, 2021.

[16] M. E. Kandel, W. Lu, J. Liang, O. Aydin, T. A. Saif, and G. Popescu. Cell-to-cell influence on growth in large populations. *Biomed. Opt. Express*, 10:4664–4675, 2019.

[17] X. Yuan, M. Zhao, X. Guo, Y. Li, Y. Yu, Z. Gan, and H. Ruan. Ultra-high capacity for three-dimensional optical data storage

inside transparent fluorescent tape. *Opt. Lett.*, 45:1535–1538, 2020.

[18] A. S. Baslamisli and T. Gevers. Invariant descriptors for intrinsic reflectance optimization. *J. Opt. Soc. Am. A*, 38:887–896, 2021.

[19] X. Fu, P. Lu, J. Zhang, Z. Qu, W. Zhang, Y. Li, P. Hu, W. Yan, W. Ni, D. Liu, and J. Zhang. Micromachined extrinsic fabry-pérot cavity for low-frequency acoustic wave sensing. *Opt. Express*, 27:24300–24310, 2019.

[20] G. Prabhakar, P. Gregg, L. Rishoj, P. Kristensen, and S. Ramachandran. Octave-wide supercontinuum generation of light-carrying orbital angular momentum. *Opt. Express*, 27:11547–11556, 2019.

[21] G. Granet and J. Bischoff. Matched coordinates for the analysis of 1d gratings. *J. Opt. Soc. Am. A.*, 38:790–798, 2021.

[22] Q. Zhu, L. Zhong, L. Yang, and X. Xu. Synthesis of the high performance yag:ce phosphor by a sol-gel method. *ECS J. Solid State Sci. Technol.*, 1:119–122, 2012.

[23] J. Wang, H. Yu, J. Shen, B. Yang, and C. Tropea. Simulation of the optical caustics associated with the primary rainbow for oblate spheroidal drops illuminated by a gaussian beam. *Opt. Express*, 29:377–384, 2021.

[24] Y. Li, X. Zhang, H. Yang, X. Yi, J. Wang, and J. Li. Effects of remote sediment phosphor plates on high power laser-based white light sources. *Opt. Express*, 29:24552–24560, 2021.

[25] Y. Fang, Y. Huang, Y. Cao, G. Zhao, Y. Liu, F. Huang, H. T. Sun, H. Ou, and J. Hou. Giant enhancement of white light emission from ca9ln(po4)7:eu2+,mn2+ (ln=la, lu, gd) phosphors achieved by remote aluminum reduction. *Opt. Mater. Express*, 10:1306–1322, 2020.

[26] H. Yuce, T. Guner, S. Balci, and M. M. Demir. Phosphor-based white led by various glassy particles: control over luminous efficiency. *Opt. Lett.*, 44:479–482, 2010.

[27] Q. Guo, M. Li, K. Yue, Y. Yan, F. Xie, C. Zhang, C. Mou, and G. D. Peng. Characterization of yag:ce phosphor dosimeter by the co-precipitation method for radiotherapy. *Appl. Opt.*, 60:3044–3048, 2021.

About Authors

Anh Tuan LE was born in Ho Chi Minh city, Vietnam. He has been working at the Faculty of Electrical and Electronics Engineering, Ton Duc Thang University. His research interests are optoelectronics and lighting design.

Hsiao-Yi LE was born in Hsinchu city, Taiwan. He has been working at the Department of Electrical Engineering, National Kaohsiung University of Science and Technology, Kaohsiung, Taiwan. His research interest is optics science.